A Classical Vacuum Spin Model for Propellantless Propulsion

Ioannis Xydous [1]

[1] BSc. E. Engineering, Piraeus, Greece, E-mail: ioannisxydous@gmail.com

A classical model of the vacuum as a continuum of massless spin carriers is developed and applied to propellantless propulsion. In this framework, a spacecraft imposes a standing electromagnetic wave with a position-dependent, time-varying phase gradient. The vacuum generates a compensating spin current, and the reaction to this induced flow produces thrust without expelling propellant. The model reproduces reported asymmetric-capacitor forces and indicates that analogous effects may arise in magnetic configurations, to be examined in future work. It also implies that a static phase gradient can reduce effective inertia by forming an "inertial bubble" that partially decouples the spacecraft interior from external acceleration. Together, these results outline a pathway from laboratory-scale devices to an inertial warp-drive concept—not by curving spacetime, but by reshaping inertia through controlled phase gradients or energy-density gradients.

DOI 10.5281/zenodo.20516763

I. INTRODUCTION

A number of reported experiments involving strong electrostatic field gradients or polarized materials—including the Exodus drive of Aurigema and Buhler [24], the Brown–Bahnson asymmetric capacitors [18, 19] as later tested by JLN Labs [14, 15], the T-shaped capacitor of Frolov [25], and the anomalous weight changes observed by Kita in polarized electrets [22]—suggest the possibility of thrust [11] or inertia modification [2, 3, 10, 12, 13, 23] without propellant. Although controversial, these results collectively point to a coupling between electromagnetic fields and vacuum structure not accounted for in standard electrodynamics. This work is motivated in part by Ivanov's Rhythmodynamics [21], which proposes that phase-shifted standing waves in the vacuum can generate force. Ivanov outlined the conceptual mechanism but did not provide a physical model describing how the vacuum interacts with a propelled object or the conditions required for sustained thrust. The present work addresses these gaps by introducing a classical model of the vacuum as a massless spin continuum obeying a spin-conservation law. In this framework, a spacecraft imposes a standing wave with a position-dependent, time-varying phase gradient. The vacuum responds by generating a compensating spin current, and the reaction to this induced flow produces thrust [1]. The same mechanism accounts for reported electrostatic thrust effects and suggests analogous behavior in magnetic configurations, which will be examined in future work. The model also implies that a static phase gradient can reduce effective inertia by forming an inertial bubble that partially decouples the spacecraft interior from external acceleration. This provides a conceptual pathway toward an inertial warp-drive concept [16, 20], achieved not by curving spacetime [5, 17] but by reshaping inertia through controlled phase gradients. In this picture, net thrust arises from the integral of a moving phase gradient over the vacuum-coupled surface. A gradient propagating from low to high field strength produces a reaction opposite to its motion; reversing the propagation direction reverses the thrust. Opposing gradients cancel, so sustained unidirectional thrust requires a net moving phase pattern with a preferred direction. Momentum conservation remains intact because the vacuum, possessing intrinsic angular momentum, serves as the reaction partner. The ability to reshape inertia through controlled phase or energy-density gradients opens a conceptual pathway toward propulsion systems unconstrained by propellant mass. Such a capability would mark a profound technological shift, enabling efficient planetary transport, rapid interplanetary transfer, and eventually the possibility of interstellar exploration.

II. CLASSICAL VACUUM SPIN MODEL

We model the vacuum as a continuum of massless spin carriers (FIG. 1), where "classical spin" denotes an intrinsic angular-momentum property of each carrier. The local spin density $\rho_s(\vec{r},t)$ and its associated flow $\vec{J}_s(\vec{r},t)$ satisfy the continuity equation

$$\frac{\partial \rho_s}{\partial t} + \nabla \cdot \vec{J}_s = 0. \tag{1}$$

expressing that spin changes only through transport across a boundary.

In SI units, the spin density ρ_s has units of angular momentum per volume ($\mathrm{kg\,m^{-1}\,s^{-1}}$), while the spin current $\vec{J}_s$ has units of angular momentum per area per time ($\mathrm{kg\,s^{-2}}$). Both terms in Eq. (1) therefore share the same dimensions, confirming consistency.

A second conservation law, derived from Poynting's theorem, parallels the spin-continuity relation. Electromagnetic energy within any region changes only through energy flow across its boundary. The differential form is

$$\frac{\partial w_s}{\partial t} + \nabla \cdot \vec{S}_s = 0. \tag{2}$$

where w_s is the electromagnetic energy density and $\vec{S}_s$ is the Poynting vector.

In SI units, w_s has units of energy per volume ($\mathrm{J\,m^{-3}}$), and $\vec{S}_s$ has units of energy per area per time ($\mathrm{W\,m^{-2}}$). The term $\partial w_s/\partial t$ measures the rate of change of stored electromagnetic

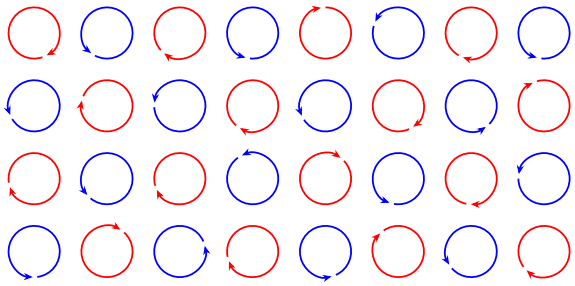

FIG. 1. **Classical vacuum illustration with massless spin.** The vacuum is modeled as a continuum of massless spin carriers (red and blue circles). Red and blue indicate opposite spin orientations, randomly distributed in the unpolarized state. The vacuum obeys the continuity equation $\frac{\partial \rho_s}{\partial t} + \nabla \cdot \vec{J}_s = 0$, meaning spin changes only by flowing across boundaries. Under acceleration, matter attempts to reorient this distribution, and the vacuum resists through continuous realignment. This reaction manifests as inertia.

energy, while $\nabla \cdot \vec{S}_s$ gives the net outward energy flow. Their sum vanishing expresses local energy conservation.

III. SPACECRAFT THRUST EQUATION

We model a spacecraft as imposing an electromagnetic standing wave with phase $\phi(\vec{r}, t)$ that varies in both space and time. The resulting phase gradient drives an energy-carrying current in the surrounding vacuum, modeled as

$$\vec{J} = \kappa \nabla \phi, \tag{3}$$

where $\kappa > 0$ (units N/rad) is the vacuum response coefficient. This current represents the imposed motion of a phase or energy-density pattern across the spacecraft surface.

The vacuum reacts to changes in this imposed flow. The reaction power density on the surface is

$$\vec{D}_{\text{thrust}} = -\frac{\partial \vec{J}}{\partial t}, \tag{4}$$

which, using the definition of $\vec{J}$, becomes

$$\vec{D}_{\text{thrust}} = -\kappa \frac{\partial}{\partial t} \nabla \phi. \tag{5}$$

Because $\vec{D}_{\text{thrust}}$ has the dimensions of a Poynting vector, we define

$$\vec{S}_{\text{vac}} \equiv \vec{D}_{\text{thrust}}, \tag{6}$$

interpreted as a vacuum reaction Poynting vector associated with the driven motion of the phase or energy-density pattern.

The net force follows from integrating the reaction flux over the interacting surface and dividing by the pattern speed u_p:

$$\vec{F}_{\text{thrust}} = \frac{1}{u_p} \int_S \vec{S}_{\text{vac}} \, dS = -\frac{\kappa}{u_p} \frac{\partial}{\partial t} \int_S \nabla \phi \, dS. \tag{7}$$

The relevant surface S is the area through which the gradient propagates: the open face in devices such as the PFT, or the exterior hull for a closed spacecraft. A spatial gradient requires no curvature; a flat electrode with a linear voltage drop already satisfies $\nabla \phi \neq 0$.

Thrust arises only when the phase varies in both space and time. The essential conditions are

$$\nabla \phi \neq 0, \qquad \frac{\partial \phi}{\partial t} \neq 0,$$

ensuring that $\partial_t \nabla \phi \neq 0$. When the gradient becomes stationary, thrust vanishes. Reversing the propagation direction reverses the force, and multiple patterns superpose vectorially.

A full phase shift of π radians transfers maximum momentum. Dividing the energy density w over the surface area $A = \int_S dS$ by π gives the vacuum response coefficient

$$\kappa = \frac{wA}{\pi}, \tag{8}$$

Substituting into Eq. (7) yields

$$\vec{F}_{\text{thrust}} = -\frac{wA}{\pi u_p} \frac{\partial}{\partial t} \int_S \nabla \phi \, dS. \tag{9}$$

An equivalent formulation uses the spatial gradient of energy density:

$$\vec{F}_{\text{thrust}} = -\frac{A}{u_p} \frac{\partial}{\partial t} \int_S \nabla w \, dS. \tag{10}$$

which links thrust directly to a moving energy-density contrast.

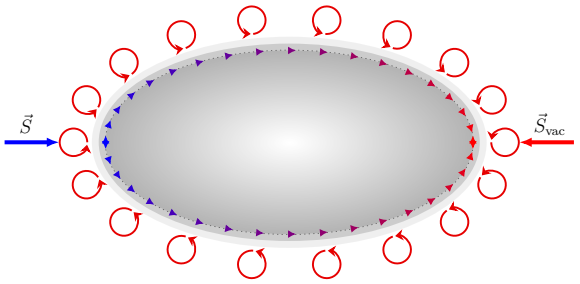

FIG. 2. **Spacecraft interaction with the vacuum.** A spatial phase gradient across the surface (blue to red) polarizes the surrounding vacuum (red circles), establishing a stored energy-density contrast. When this gradient subsequently varies in time, the phase or energy-density pattern propagates across the surface, giving rise to a Poynting vector $\vec{S}$ associated with the moving pattern. As the gradient advances, the vacuum releases the momentum accumulated during the earlier polarization, producing a reaction flow $\vec{S}_{\text{vac}}$ opposite to the direction of propagation. The illustration represents the case in which the spacecraft's inertia is directly coupled to the thrust mechanism, so that both act as a single system interacting with the vacuum.

For open structures, ∇w propagates across the open face; for closed structures, the interaction occurs over the hull. Eq. (10) parallels the classical electrodynamic expression

$$\vec{F}_{\text{field}} = \frac{1}{c^2} \frac{d}{dt} \int_V \vec{S} \, dV.$$

where $\vec{S}$ is the electromagnetic Poynting vector. In analogy, $\vec{S}_{\rm vac}$ represents the momentum exchange between the driven gradient pattern and the vacuum, with the reaction directed back onto the spacecraft surface.

IV. ORIGIN OF INERTIA

The response coefficient κ quantifies the coupling between the spacecraft and the vacuum structure. In this model, inertia arises not only from the intrinsic rest energy mc^2 but also from the interaction between matter and the vacuum's random angular-momentum polarization. In its natural isotropic state, the vacuum polarization opposes changes in motion, giving rise to ordinary inertial reaction.

A static spatial structure—represented by a stationary gradient of electromagnetic energy density—partially aligns the vacuum polarization. Establishing this alignment requires work, since the initially random spin distribution must be reoriented. The required energy is drawn from the electromagnetic field, reducing the spacecraft's effective electromagnetic inertia. The missing energy resides in the aligned vacuum configuration, so the reduction reflects a change in the vacuum's opposition to acceleration rather than a change in rest mass.

Let the vacuum have energy density w_0. With no imposed gradient, the energy in volume V is $U_0 = w_0 V$. Establishing a static energy-density gradient requires alignment energy $U_{\rm align}$, giving

$$U_{\rm total} = U_0 + U_{\rm align}. \tag{11}$$

For a closed spacecraft–vacuum system, total energy is conserved:

$$U_{\rm sc} + U_0 = \text{constant}, \tag{12}$$

so when the vacuum gains $U_{\rm align} > 0$, the spacecraft loses the same amount:

$$\Delta U_{\rm sc} = -U_{\rm align}, \tag{13}$$

If the spacecraft's effective inertia is proportional to the energy available to resist acceleration, the corresponding mass change is

$$\Delta m = -\frac{U_{\rm align}}{u_0^2}, \tag{14}$$

where u_0 is the propagation speed of vacuum excitations (equal to c only if Lorentz symmetry holds).

For a static configuration, the alignment energy must depend on the structure of the energy-density gradient over the entire enclosing surface. The appropriate quantity is the surface integral

$$W_\nabla = \int_S |\nabla w|\, dS, \tag{15}$$

which measures the total imposed contrast of energy density across the spacecraft boundary. The absolute value ensures that regions of opposite orientation contribute positively, since inertia reduction depends on the magnitude of alignment rather than its direction.

The alignment energy associated with a given surface-integrated gradient is

$$U_{\rm align} = \frac{1}{2}\,\zeta\, W_\nabla, \tag{16}$$

where ζ is a vacuum response coefficient. Let $W_{\nabla,\max}$ denote the maximum attainable surface-integrated gradient. The corresponding maximum alignment energy is

$$U_{\rm align,max} = \frac{1}{2}\,\zeta\, W_{\nabla,\max}, \tag{17}$$

Assuming linear response, the effective inertia-reduction relation becomes

$$\frac{\Delta m}{m} = -\frac{U_{\rm align}}{U_{\rm align,max}} = -\frac{W_\nabla}{W_{\nabla,\max}}, \tag{18}$$

so the effective inertial mass is

$$m_i = m\left(1 - \frac{W_\nabla}{W_{\nabla,\max}}\right). \tag{19}$$

Uniform shielding requires ∇w to be constant over the enclosed surface. A uniformly charged sphere produces no gradient; a constant gradient on a closed surface requires a linearly varying field strength, which can be approximated using segmented electrodes. The patent by R. Kita [22] describes an organic dielectric whose electron configuration changes under applied fields. In the present model, this corresponds to establishing a static gradient that reduces the material's effective inertia rather than altering gravitational coupling.

The electromagnetic surface encloses the spacecraft, forming a bubble that isolates the interior from external random polarization. All enclosed matter shares the same reduced inertia, so during acceleration the crew experiences no inertial forces.

A two-step process follows. First, a strong static gradient ∇w is established to create the inertial bubble. Second, with the gradient held constant, the reduced inertial mass m_i allows large accelerations from small external forces. To stop or change direction, the gradient is removed or reversed.

Momentum is conserved: the missing momentum resides in the aligned vacuum configuration. When the gradient is removed, the vacuum returns to its random state and releases this stored momentum as thrust. The stored momentum is

$$p_{\rm stored} = (m - m_i)v = m\frac{W_\nabla}{W_{\nabla,\max}}v, \tag{20}$$

and the resulting impulse is

$$\int \vec{F}_{\rm thrust}\, dt = \vec{p}_{\rm stored}. \tag{21}$$

The shielding energy available is $U_{\rm align,max}$. Comparing this to the spacecraft's equivalent energy $U_{\rm align,sc}$ determines the degree of shielding: $U_{\rm align,max} < U_{\rm align,sc}$ gives partial

shielding, $U_{\text{align,max}} = U_{\text{align,sc}}$ gives full shielding ($m_i = 0$), and $U_{\text{align,max}} > U_{\text{align,sc}}$ allows over-shielding. The ratio $U_{\text{align,max}}/U_{\text{align,sc}}$ bounds m_i between 0 and m. Negative inertia cannot occur because the available electromagnetic energy is finite.

This framework naturally explains why some experiments report transient effects but no steady-state mass change. The experiments of Mikhailov [10, 12, 23], inspired by the earlier proposals of Assis [2, 3], attempted to measure mass reduction inside a charged spherical shell. Assis, using Weber electrodynamics [4], obtained $m_i = m(1 - qV_E/3c^2)$. Mikhailov reported positive results, but independent replications found no steady-state effect.

Within the present model, this discrepancy is explained by transients. When the sphere is first charged, the charge distribution is non-uniform and evolves toward equilibrium. During this interval, the moving charge produces a time-varying energy-density gradient $\partial_t \nabla w \neq 0$, temporarily reducing inertia. Once the distribution becomes uniform, the gradient vanishes and the effect disappears. Most replications measured only the steady state, explaining the null results. Sustained inertia reduction requires a non-uniform or segmented charge distribution to maintain a constant gradient across the surface.

V. CAPACITOR THRUSTER

The transient mechanism identified in the Mikhailov experiment applies directly to electrostatic propellantless thrusters whose operation depends on vacuum interaction rather than ion wind. Relevant examples include the Exodus Drive [24], the Brown–Bahnson asymmetric capacitors [15, 19], Frolov's T-capacitors [14, 25], and the Poynting Flow Thruster (PFT) [6–9].

The PFT, introduced by Jean-Louis Naudin in 1999, demonstrates measurable thrust from a symmetric parallel-plate capacitor. Tests performed in sealed containers confirmed that the effect persists without airflow, ion wind, or convection, indicating that the reaction partner is the vacuum.

In the PFT, thrust appears only during charging and discharging transients, when a time-dependent spatial gradient of electromagnetic energy density exists. The dielectric increases the stored energy density, amplifying the effect. Within the present model, this behavior follows from Eqs. (7) and (10): a moving energy-density gradient interacts with the vacuum, and the reaction to this flow produces force.

— PFT Parallel Plate Capacitor — Based on J. L. Naudin's Experiment [7]:

- Dielectric: Plexiglas, thickness $d = 0.001$ m
- Aluminum plates: 0.12×0.11 m
- Plate length $L = 0.12$ m, width $W = 0.11$ m
- Plate separation: $d = 0.001$ m
- Dielectric constant: $\varepsilon_r \approx 3.4$
- Applied voltage: $V_0 = 30$ kV

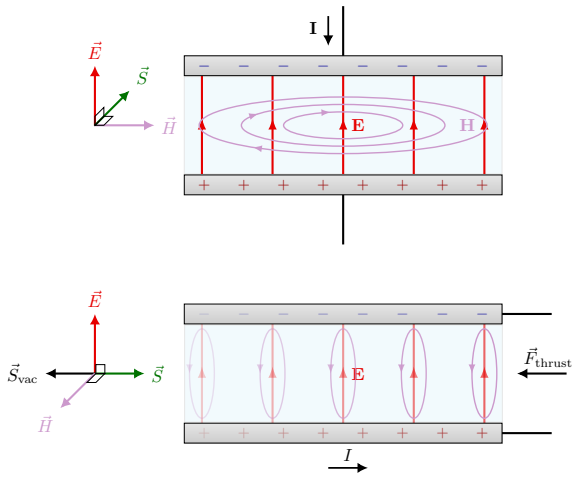

FIG. 3. **Capacitor thruster mechanism.** The top illustration shows a uniformly charging capacitor, where the Poynting vector points inward symmetrically and no thrust arises. The bottom illustration shows the transient charging phase when the plates are fed from their edges: a surface current spreads across the plates, generating a magnetic field $\vec{H}$ throughout the dielectric. During this interval, the Poynting vector $\vec{S}$ follows the current flow, producing a moving energy-density gradient. The vacuum responds with an opposing reaction flow $\vec{S}_{\text{vac}}$, yielding a thrust force $\vec{F}_{\text{thrust}}$ opposite to $\vec{S}$.

- Wire connection: HV and ground wires attached 10 mm from the plate edge
- Capacitance: $C = 15$ pF, stored energy $U = 6.5$ mJ
- Rise time: $\Delta t_1 = 1$ s (estimated)
- Total mass: $m = 0.02$ kg (estimated)

— Electric field and energy density at the wire edge:

$$E = V_0/d = 3 \times 10^7 \text{ V/m}, \quad w = \frac{1}{2}\varepsilon_0 \varepsilon_r E^2 \approx 1.35 \times 10^4 \text{ J/m}^3.$$

— Energy density at the opposite edge:

$$w_{\text{far}} \approx 0.$$

— Spatial gradient of energy density:

$$|\nabla w| \approx \frac{1.35 \times 10^4}{0.12} \approx 1.125 \times 10^5 \text{ J/m}^4.$$

— Interacting surface (open side face):

$$A_{\text{cross}} = W \times d = 1.1 \times 10^{-4} \text{ m}^2.$$

— Flux of ∇w through the open surface with efficiency η:

$$\Phi \approx \eta |\nabla w| A_{\text{cross}} \approx 6.18 \text{ J/m}^2, \qquad \eta = 0.5.$$

— Time derivative of the flux:

$$u_p = L/\Delta t_1 = 0.12 \text{ m/s}, \qquad \frac{\partial \Phi}{\partial t} \approx 6.19 \text{ W/m}^2.$$

— *Peak thrust*:

$$F_{\text{peak}} = -\frac{A_{\text{cross}}}{u_p}\frac{\partial \Phi}{\partial t} \approx -5.6\,\text{mN}.$$

This peak force is independent of the rise time; only the pulse duration changes. A rapid discharge produces a much smaller reverse impulse, enabling net unidirectional thrust.

— *Charging phase* ($\Delta t_1 = 1$ s):

$$m\Delta v_1 = \frac{1}{2}F_{\text{peak}}\Delta t_1 = -2.8\times10^{-3}\,\text{N·s}, \qquad \Delta v_1 = -0.14\,\text{m/s}.$$

— *Discharging phase* ($\Delta t_2 = 1$ ms):

$$m\Delta v_2 = \frac{1}{2}F_{\text{peak}}\Delta t_2 = 2.8\times10^{-6}\,\text{N·s}, \qquad \Delta v_2 = 1.4\times10^{-4}\,\text{m/s}.$$

— *Net impulse per cycle*:

$$\Delta p_{\text{net}} = m\Delta v_1 + m\Delta v_2 \approx -2.8\times10^{-3}\,\text{N·s}.$$

— *Average thrust*:

$$F_{\text{avg}} = \frac{\Delta p_{\text{net}}}{\Delta t} \approx -2.8\,\text{mN}, \qquad \Delta t = \Delta t_1 + \Delta t_2.$$

— *Thrust-to-power ratio*:

$$P_{\text{avg}} = U/\Delta t, \qquad \frac{|F_{\text{avg}}|}{|P_{\text{avg}}|} \approx 0.43\,\text{N/W}.$$

This high thrust-per-watt ratio arises because the vacuum reaction couples directly to the moving energy-density gradient rather than to expelled mass or an external medium.

— *Mechanism*: In the PFT, both the high-voltage and return leads connect near the same plate edge (FIG. 3), producing asymmetric energy entry. The top illustration shows the idealized case of symmetric feeding, where $\vec{S}$ is inward and no thrust occurs. In the actual device, charging begins at the plate edges. A surface current spreads across the plates, generating a magnetic field throughout the dielectric and producing a directed Poynting flux.

This edge-driven redistribution defines the transient regime. Electrons move toward regions of higher potential, generating a time-varying energy-density gradient ($\partial_t \nabla w \neq 0$). The direction of this moving gradient coincides with $\vec{S}$, and the vacuum responds with an opposing reaction flow $\vec{S}_{\text{vac}}$, yielding a thrust force $\vec{F}_{\text{thrust}}$ opposite to $\vec{S}$. The bottom illustration of FIG. 3 depicts this state just before the charge becomes uniform.

Once the voltage stabilizes and the plates reach uniform charge, the gradient vanishes and thrust drops to zero. Each new voltage increase initiates another transient. During discharge, the gradient reverses and a counter-thrust is produced. To obtain net forward thrust, this reverse impulse must be minimized. A sawtooth waveform naturally provides the required asymmetry: the slow voltage rise produces a long forward impulse, while the rapid discharge yields only a brief counter-thrust, resulting in net unidirectional force.

VI. DISCUSSION

Having established the thrust and inertia mechanisms in the preceding sections, we now examine their broader physical implications and the experimental evidence supporting vacuum–structure interaction.

— *Vacuum coupling cannot be shielded*: Because the vacuum permeates all matter, including the empty space within atoms, it cannot be excluded by any material enclosure. This raises the question of whether a thrust mechanism placed inside a sealed container would experience internal force cancellation, as classical mechanics predicts for a closed system. Within the present framework, the answer is negative: the reaction partner is not the enclosing mass but the vacuum itself, which exists both inside and outside any boundary. Consequently, shielding the vacuum coupling with a massive enclosure is impossible.

Experimental results support this conclusion. JLN Labs tested both Frolov's Hat [14] and the Poynting Flow Thruster (PFT) [6] inside sealed bags to eliminate airflow or ion-wind effects. Thrust persisted despite the enclosure, indicating that the reaction arises from the vacuum rather than from interaction with the surrounding medium. This behavior parallels that of closed-cavity devices such as the EM Drive, where electromagnetic energy has no exhaust path yet thrust is still reported. In all such cases, the vacuum remains the only viable reaction partner.

Because the vacuum cannot be shielded, a propulsion mechanism may operate entirely within a closed structure, including the interior of a spacecraft. This implies that propellantless propulsion could, in principle, enable maneuverable vehicles operating within Earth's atmosphere at limited velocities without requiring external reaction mass.

— *Vacuum reaction to the Poynting vector*: In the PFT, the asymmetric placement of both leads near the same plate edge produces a transient, not static, field configuration. As charge spreads across the plate, it generates propagating electric and magnetic fields, forming a traveling electromagnetic pattern. This moving charge front constitutes a current, and the combined $\vec{E}$ and $\vec{H}$ fields produce a translating energy-density distribution—a frozen wave that shifts across the dielectric region.

The Poynting vector $\vec{S} = \vec{E} \times \vec{H}$ points from the feed edge toward the opposite side, following the direction of the advancing gradient. Under a sawtooth driving voltage, this pattern advances progressively while maintaining its shape. Such a translating static pattern is the essential condition for thrust: the vacuum resists the motion of the energy-density gradient, producing a reaction force opposite to $\vec{S}$. Thrust therefore emerges as an anti-Poynting-vector effect.

This interpretation is consistent with Y. N. Ivanov's Rhythmodynamics [21]. Ivanov recognized that a translating standing-wave pattern could serve as a propulsion mechanism in vacuum but did not specify how such a wave interacts with the vacuum to produce force. The present model provides the missing link by identifying the translating energy-density gradient and the vacuum's opposition to it as the fundamental origin of thrust.

VII. INERTIAL WARP DRIVE

The concept of a warp drive is most widely associated with the Alcubierre metric, a general-relativistic solution in which spacetime is engineered to contract in front of a spacecraft and expand behind it. Propulsion is achieved not by accelerating the craft through space, but by deforming the spacetime geometry around it. Although consistent with Einstein's field equations, such configurations require exotic stress–energy distributions and remain far beyond known physical capabilities.

In contrast to general-relativistic warp drives that deform spacetime, an inertial warp drive modifies the spacecraft's inertial response by engineering its interaction with the vacuum. Rather than bending the metric, the mechanism reshapes the effective inertia within a controlled region surrounding the craft.

This effect is produced (FIG. 2) by imposing a spatial phase gradient across the surface. Once established, the surrounding vacuum becomes polarized. When the gradient then varies in time, the phase or energy-density pattern propagates across the surface, generating a Poynting vector $\vec{S}$ associated with the moving pattern. As this advancing gradient releases the momentum stored during the earlier polarization, the vacuum responds with a counter-flow $\vec{S}_{\rm vac}$ directed opposite to the propagation.

A natural question arises: would such a mechanism violate Einstein's framework of special relativity, particularly its connection between velocity and increasing inertia? Before deriving the mathematical extension of the theory, it is useful to recall the physical picture.

In the section on the origin of inertia, we saw that inertia—the resistance of matter to acceleration—emerges from the vacuum's reaction to changes in motion. By imposing a spatial energy-density gradient, this vacuum reaction can be reduced, lowering the inertial response of the spacecraft.

Without such polarization, the inertia of a body increases with speed, as dictated by Einstein's formulation. But with a controllable reduction of inertia, the situation reverses: the effective inertia can *decrease* as speed increases. If the resistance to acceleration diminishes rather than grows, the usual relativistic barrier loses its foundation.

This leads to an important question: if inertia can be engineered downward as velocity rises, does the notion of a fundamental speed limit still hold?

Based on the previously derived inertia expression (Eq. (19)), we now clarify how the inertial mass m appears in

$$m_i = m\left(1 - \frac{W_\nabla}{W_{\nabla,\max}}\right) = m\left(1 - \frac{U_{\rm align}}{U_{\rm align,max}}\right). \tag{22}$$

When inertia is coupled to the vacuum, the expression indicates that it is tied to a specific energy scale $U_{\rm align,max}$, which in turn implies an association with the interaction surface enclosing the spacecraft. There must therefore exist a baseline energy that scales with the effective interaction area—an energy scale that, together with u_0, must ultimately be determined either experimentally or theoretically.

Furthermore, $U_{\rm align,max}$ represents the maximum attainable alignment permitted by the spacecraft's available stored energy.

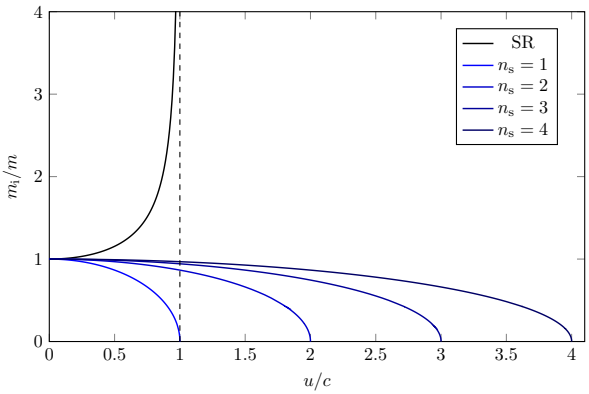

FIG. 4. **Relativistic inertia.** In special relativity (SR), the inertial mass m_i increases with speed u, diverging as u approaches the speed of light c. In contrast, when inertia reduction is applied in synchrony with the increasing velocity, the effective inertia m_i can decrease with u, reaching zero and permitting velocities u that may exceed the speed of light c.

This value may be larger or smaller than the shielding energy $U_{\rm align,sc}$ required for the spacecraft.

We consider an ellipsoidal spacecraft, as illustrated in FIG. 2. Its structure may consist of a single functional layer, in which propulsion and inertial shielding operate in parallel, or of two distinct layers: an outer shell dedicated to propulsion and an inner shell used exclusively for inertial shielding, ensuring continued protection if propulsion ceases.

Starting with the Minkowski line element,

$$ds^2 = -c^2dt^2 + dx^2 + dy^2 + dz^2, \tag{23}$$

and assuming motion only along the x–direction, this reduces to

$$ds^2 = -c^2dt^2 + dx^2. \tag{24}$$

To incorporate the inertia-reduction effect into the metric, we scale the line element by $(m_i/m)^2$ and introduce an additional scaling n_s^2 to represent the maximum available stored energy. This yields

$$ds^2 = -n_s^2c^2d\tau^2\left(\frac{m_i}{m}\right)^2, \tag{25}$$

Applying the same scaling to the coordinate form of the metric gives

$$ds^2 = -n_s^2c^2dt^2 + n_s^2dx^2, \tag{26}$$

Using the kinematic relation $n_s\,dx = u\,dt$, we obtain

$$ds^2 = -n_s^2c^2dt^2 + u^2dt^2, \tag{27}$$

Relating this to the proper time expression,

$$-n_s^2c^2d\tau^2\left(\frac{m_i}{m}\right)^2 = \left[-n_s^2c^2 + u^2\right]dt^2, \tag{28}$$

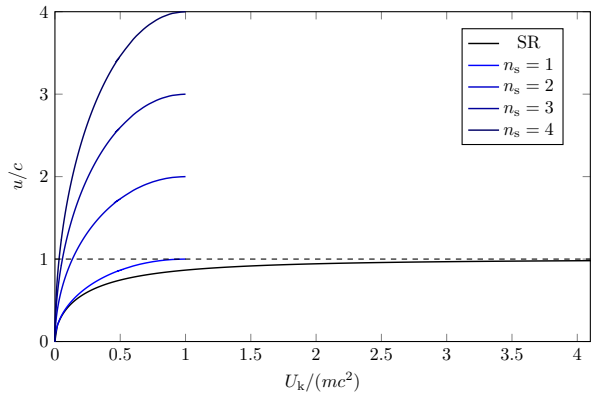

FIG. 5. **Relativistic velocity.** In SR, the kinetic energy may increase without bound, yet the velocity never exceeds c. With synchronized inertia reduction, the effective light-speed barrier becomes $n_s c$, allowing velocities beyond c when $n_s > 1$.

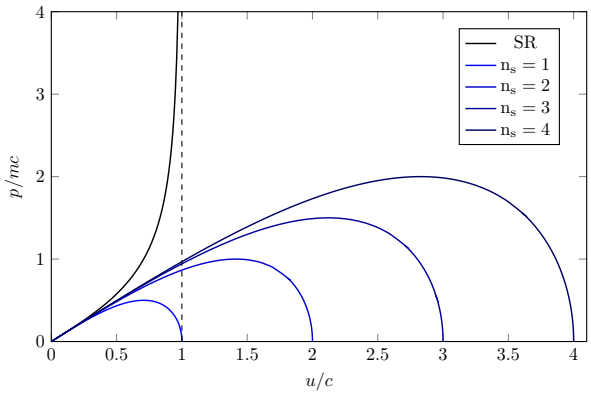

FIG. 6. **Relativistic momentum.** In SR, momentum diverges as velocity increases. With synchronized inertia reduction, momentum rises, peaks, and then decreases to zero as the effective inertia vanishes.

Dividing by $-n_s^2 c^2$ yields

$$d\tau^2 \left(\frac{m_i}{m}\right)^2 = \left[1 - \frac{u^2}{n_s^2 c^2}\right] dt^2, \tag{29}$$

from which we obtain

$$\frac{dt}{d\tau} = \left(\frac{m_i}{m}\right) \frac{1}{\sqrt{1 - \frac{u^2}{n_s^2 c^2}}}. \tag{30}$$

The relation between the stored energy $U_{\text{align,max}}$ and the scaling factor n_s is

$$\frac{U_{\text{align}}}{U_{\text{align,max}}} = \frac{U_{\text{align}}}{n_s U_{\text{align,sc}}}, \tag{31}$$

which gives

$$\frac{m_i}{m} = 1 - \frac{U_{\text{align}}}{n_s U_{\text{align,sc}}}. \tag{32}$$

Thus the ratio between coordinate time dt and proper time $d\tau$ becomes

$$\frac{dt}{d\tau} = \left(1 - \frac{U_{\text{align}}}{n_s U_{\text{align,sc}}}\right) \frac{1}{\sqrt{1 - \frac{u^2}{n_s^2 c^2}}}. \tag{33}$$

— *Relativistic energy*: The relativistic energy follows as

$$m_i c^2 = mc^2 \left(1 - \frac{U_{\text{align}}}{n_s U_{\text{align,sc}}}\right) \frac{1}{\sqrt{1 - \frac{u^2}{n_s^2 c^2}}}. \tag{34}$$

When no energy-density gradient is imposed ($U_{\text{align}} = 0$ and $n_s = 1$), this reduces to the familiar special-relativistic expression.

When the propulsion system that couples to the vacuum is activated, the two ratios—the inertia-reduction energy ratio and the velocity ratio—may operate independently (two-layer configuration) or in synchrony (single-layer configuration). In both cases this yields

$$\frac{U_{\text{align}}}{n_s U_{\text{align,sc}}} = \frac{u^2}{n_s^2 c^2}. \tag{35}$$

Assuming that the time-varying energy-density gradient arises from the moving pattern of a standing wave, whose velocity is determined by a time-dependent phase $\phi(t)$, we apply a phase-dependent velocity similar to that in Ivanov's Rhythmodynamics:

$$u = n_s c \, \frac{\phi(t)}{\pi}, \tag{36}$$

The relativistic energy (FIG. 4) then becomes

$$m_i c^2 = mc^2 \sqrt{1 - \frac{u^2}{n_s^2 c^2}}. \tag{37}$$

For $n_s = 1$, this reproduces the expression obtained by R. L. Carezani [20]:

$$m_i c^2 = mc^2 \sqrt{1 - \frac{u^2}{c^2}}. \tag{38}$$

Although Carezani did not discuss inertia reduction, his reduction of inertial frames to a single effective frame resembles, at a conceptual level, the coupling between the inertial-shielding energy ratio and the velocity ratio in our framework.

— *Relativistic velocity*: In standard relativity,

$$U_k = m_i c^2 - mc^2 = mc^2 \left(\frac{1}{\sqrt{1 - \frac{u^2}{c^2}}} - 1\right), \tag{39}$$

leading to

$$u = c \sqrt{1 - \left(\frac{1}{1 + \frac{U_k}{mc^2}}\right)^2}. \tag{40}$$

In the modified framework,

$$-U_k = m_i c^2 - mc^2 = mc^2 \left(\sqrt{1 - \frac{u^2}{n_s^2 c^2}} - 1 \right), \tag{41}$$

yielding the velocity–energy relation (FIG. 5)

$$u = n_s c \sqrt{1 - \left(1 - \frac{U_k}{mc^2}\right)^2}. \tag{42}$$

— *Relativistic momentum*: In standard relativity,

$$p = \frac{mu}{\sqrt{1 - \frac{u^2}{c^2}}}. \tag{43}$$

In the modified framework (FIG. 6),

$$p = mu \sqrt{1 - \frac{u^2}{n_s^2 c^2}}. \tag{44}$$

VIII. CONCLUSION

The model developed here treats the vacuum as a continuum of massless spin carriers capable of exchanging momentum with electromagnetic phase structures. Within this framework, a translating phase gradient acts as the fundamental agent of propulsion: the vacuum generates a compensating spin flow, and the reaction to this induced motion produces thrust without propellant. This mechanism accounts for reported electrostatic anomalies and provides a unified physical picture in which thrust, inertia reduction, and phase-controlled energy flow arise from the same underlying interaction. A static phase or energy-density
decouples the spacecraft interior from external acceleration, while a moving gradient produces a reaction force determined by the direction and magnitude of the phase shift. Because the vacuum permeates all matter, this coupling cannot be shielded, allowing propulsion to operate entirely within closed structures. Momentum conservation is preserved by identifying the vacuum itself as the reaction partner. The present work establishes the theoretical foundation for this mechanism and clarifies the conditions under which it can generate measurable thrust. Extending the analysis to magnetic configurations and maturing the underlying engineering principles may enable a new class of propulsion technologies that scale from laboratory prototypes to planetary and interplanetary vehicles, and eventually to architectures capable of supporting interstellar exploration.

[1] I. Newton, *Philosophiæ Naturalis Principia Mathematica*, Royal Society, 1687.

[2] A. K. T. Assis, *Weber's law and mass variation*, Physics Letters A, 1989, 136, 277–280.

[3] A. K. T. Assis, *Changing the Inertial Mass of a Charged Particle*, Journal of the Physical Society of Japan, 1993, 62, 1418–1422.

[4] A. K. T. Assis, *Weber's Electrodynamics*, Kluwer Academic, 1994, 10.1007/978-94-017-3670-1.

[5] M. Alcubierre, *The warp drive: hyper-fast travel within general relativity*, Classical and Quantum Gravity, 1994, 10.1088/0264-9381/11/5/001.

[6] J.-L. Naudin, *The PFT Proof of Concept*, JLN Labs, 1999, JLN Labs.

[7] J.-L. Naudin, *The PFT v1.0*, JLN Labs, 1999, JLN Labs.

[8] J.-L. Naudin, *The PFT v2.0*, JLN Labs, 1999, JLN Labs.

[9] J.-L. Naudin, *The PFT v3.0*, JLN Labs, 1999, JLN Labs.

[10] V. F. Mikhailov, *The Action of an Electrostatic Potential on the Electron Mass*, Annales de la Fondation Louis de Broglie, 1999.

[11] S. G. Dimitriou, *Efforts in developing upward and directional thrust*, Presented at the Propellantless Propulsion Conference, University of Sussex, 2001.

[12] V. F. Mikhailov, *Influence of an electrostatic potential on the inertial electron mass*, Annales de la Fondation Louis de Broglie, 2001.

[13] J. P. Wesley, *Inertial Mass Energy Equivalence*, Physics Essays, 2001.

[14] J.-L. Naudin, *The ELG Frolov's Hat experiment*, JLN Labs, 2000, JLN Labs.

[15] J.-L. Naudin, *The Brown-Bahnson Thruster*, JLN Labs, 2002, JLN Labs.

[16] A. Einstein, *On the Electrodynamics of Moving Bodies*, Annalen der Physik, 1905.

[17] A. Einstein, *The Field Equations of Gravitation*, Akademie der Wissenschaften zu Berlin, 1915.

[18] T. T. Brown, *Electrokinetic apparatus*, U.S. Patent 3,187,206, 1965, US3187206.

[19] A. H. Bahnson, Jr., *Electrical thrust producing device*, U.S. Patent 3,227,901, 1966, US3227901.

[20] R. L. Carezani, *Autodynamics: Fundamental Basis for a New Relativistic Mechanics*, SAA Publications, 1998. ISBN 978-0966553307.

[21] Y. N. Ivanov, *Rhythmodynamics*, 2nd Edition, Energia Publishing, 2007. ISBN 978-5-98420-018-9.

[22] R. Kita, *Gravitational attenuating material*, U.S. Patent 8,901,943, 2014, US8901943.

[23] M. Weikert and M. Tajmar, *Investigation of the Influence of a field-free electrostatic Potential on the Electron Mass with Barkhausen-Kurz Oscillation*, Annales de la Fondation Louis de Broglie, 2019, 44, 23–38.

[24] C. R. Buhler and A. N. Aurigema, *System and method for generating forces using asymmetrical electrostatic pressure*, WIPO Patent WO2020159603A2, 2020, WO2020159603A2.

[25] A. V. Frolov, *Propulsion device based on an asymmetric capacitor*, Faraday.ru, 2024, T-Cap.